A novel respiration pattern biometric prediction system based on artificial neural network

Rafiu King Raji
Department of fashion Engineering, Glorious Sun Guangdong Fashion College, Huizhou University, Huizhou, China
Michael Adjeisah
School of Information Science and Technology, Donghua University, Shanghai, China
Xuhong Miao
Engineering Research Center of Knitting Technology, Ministry of Education, Jiangnan University, Wuxi, China, and
Ailan Wan
Engineering Research Center of Knitting Technology, Ministry of Education, Jiangnan University, Wuxi, China; Key Laboratory of Advanced Textile Materials and Manufacturing Technology, Ministry of Education, Zhejiang Sci-Tech University, Hangzhou, China and Key Laboratory of Textile Fiber and Product, Ministry of Education, Wuhan Textile University, Wuhan, China

Abstract

Purpose – The purpose of this paper is to introduce a novel respiration pattern-based biometric prediction system (BPS) by using artificial neural network (ANN).

Design/methodology/approach – Respiration patterns were obtained using a knitted piezoresistive smart chest band. The ANN model was implemented by using four hidden layers to help achieve the best complexity to produce an adequate fit for the data. Not only did this study give a detailed distribution of an ANN model construction including the scheme of parameters and network layers, ablation of the architecture and the derivation of back-propagation during the iterations but also engaged a step-based decay to systematically drop the learning rate after specific epochs during training to minimize the loss and increase the model's accuracy as well as to limit the risk of overfitting.

Findings – Findings establish the feasibility of using respiratory patterns for biometric identification. Experimental results show that, with a learning rate drop factor = 0.5, the network is able to continue to learn past epoch 40 until stagnation occurs which yielded a classification accuracy of 98 per cent. Out of 51,338 test set, the model achieved 51,557 correctly classified instances and 169 misclassified instances.

Practical implications – The findings provide an impetus for possible studies into the application of chest breathing sensors for human machine interfaces in the area of entertainment.

Originality/value – This is the first time respiratory patterns have been applied in biometric prediction system design.

Keywords Sensors, Biometrics, Machine intelligence, Neural networks, Force sensing, Artificial neural network, Biometric prediction system, Knitting, Strain sensor, Smart wear

Paper type Research paper

1. Introduction

Biometrics describes the collection of human distinctive, measurable characteristics with the intent to distinguish, verify or authenticate individuals. The most commonly collected biometric features are fingerprints, hand geometry, face, eye/iris/retina and voice. Even though these biometric forms have achieved enormous successes and found applications in numerous fields, spoof attacks (Ring, 2015) have been one of the major bottlenecks. This has led to continuous studies to unearth more robust biometric systems that are more resilient to spoof attacks.

Two main approaches have been adopted to fight spoof attacks in biometric technology, namely, adoption of obtrusive biometric features and multimodal biometrics. The multimodal biometrics concept uses a multi-factor identification or authentication method where multiple features are extracted for identification or authentication as opposed to a single factor in the "classic" unimodal biometric systems (Gilady *et al.*, 2014). In the case of obtrusive biometrics, features extracted require active participation of the user and tend to recognize liveness rather than static features.

Several studies, prototype systems and even commercial products have featured these two approaches. Multimodal

The current issue and full text archive of this journal is available on Emerald Insight at: **https://www.emerald.com/insight/0260-2288.htm**

Sensor Review
40/1 (2020) 8–16
© Emerald Publishing Limited [ISSN 0260-2288]
[DOI 10.1108/SR-10-2019-0235]

Conflicts of Interest: The authors declare that there is no conflict of interest regarding the publication of this article.

Received 1 October 2019
Revised 5 February 2020
Accepted 9 February 2020

applications include combining multiple fingerprints (Khuwaja, 2006), face plus fingerprint and electrocardiogram (ECG), finger geometry plus knuckle print and palm print and several other combinations involving known biometric systems. Obtrusive systems include the use of physiological signals, such as electroencephalogram (EEG) (Campisi and Rocca, 2009), ECG (Biel *et al.*, 2001) and heart rates (Akhter *et al.*, 2016). An EEG is a test that detects electrical activity in the brain using small, metal discs (electrodes) attached to your scalp, whereas an ECG is a recording of time-varying bio-electric potential generated by the electrical activity of the heart (Singh *et al.*, 2012). Liveness detection in fingerprint systems has also been applied as a means of spoof detection.

We hypothesized that that breath patterns, just like the other known physiological signals, such as ECG and EEG, can be used as biometric feature for authentication. There has however been no research report on the use respiration data for biometric identification even though its data is akin to the other physiological parameters, such as ECG and EEG. Respiratory measurement or respiratory tests describes a series of tests that measures the amount of air in one's lungs, i.e. the amount of air inhaled into the lungs and the amount of air exhaled from the lungs and at what rate. This phenomenon affords enough oxygen supply to meet the energy production requirements of the body and maintain a suitable acid-base condition by releasing carbon dioxide from the body.

Several technologies have been used to measure respiration and they include manual modes like physical counting through auscultation to advance automated tests like spirometry (Sharpton *et al.*, 2019), pneumography (Wilkinson and Thanawala, 2009), plethysmography (Rétory *et al.*, 2017) or oximetry (Kirson and Koltes-Edwards, 2011), acoustic (Mimoz *et al.*, 2012), photoplethysmography (Macwan *et al.*, 2019), capnography (Duke, 2011), accelerometry (Lapi *et al.*, 2014) and derivations from other physiological measurements, such as phonocardiography (Cheema and Singh, 2019), ECG and heart rate. The test results vary slightly depending on the equipment used or and the intended application of result.

This paper thus presents new approach in human identification using respiration patterns adduced from a knitted piezoresistive smart chest band (KTC Respiration Sensor) (Raji *et al.*, 2019). The working of the smart band is such that during inspiration the cross-sectional area of the rib cage and abdomen increases altering the resistance of the sensitive section and the frequency of their oscillation, with the increase in cross-sectional area proportional to lung volumes. The respiration indicators measured by the system include respiration cycle, respiration rate (RR), inspiratory duty cycle (DTCY), breath volume (BV) and moment ventilation (MV).

Using artificial neuron network (ANN) computational model, features were extracted and used to train the system to identify users. ANNs works such that they model the biological neural networks in the brain and have been proven effective for classification and categorization, prediction, pattern recognition and control applications (Sibai *et al.*, 2011). Several types of ANNs exist in literature and they include feedforward neural networks, radial basis function networks, Kohonen self-organizing networks, stochastic neural networks, recurrent networks, convolutional neural networks, dynamic neural networks, modular neural networks, cascading neural networks, neuro-fuzzy networks and multi-layer perceptron neural networks (Sibai *et al.*, 2011). The use of these neural networks for biometric prediction systems has been presented by a number of researchers. An ANN has several advantages but one of the most recognized of these is the fact that it can actually learn from observing data sets.

2. Experimental

The proposed system operates by acquiring respiration information from an end user. This is followed by processing, training and testing, building of ANN model, setting the learning rates and finally prediction of user's identity. Deciding how well they match and indicating whether or not an identification or verification has been achieved ends the process. Figure 1 shows the flow chart of the system's working process.

3. Methodology

3.1 Capturing of data

A total of ten users were tested under several three main test conditions including standing and sitting posture while reading. During testing, the length of the conductive section of the band was measured before and after being worn by the user. This was done to ensure that tightness is even for all users irrespective of body size.

Smart band was strapped around the chest of the user and connected with the processing box. Figure 2(a) shows the smart chest band and its signal acquisition, processing and transmission components. The knitted band is the sensing unit, the signal acquisition, processing and transmission system (processing box) is attached to the band during respiration assessment test and signals transmitted wirelessly (Bluetooth) to a computer for display and analysis.

The test interface designed using Visual Studio 2012 is presented in Figure 2(b); it entails a panel to enter name and age of the user, signal display range and the resistance of the sensor. A start button and a pause/resume button and a replay button to replay the latest test which is recorded automatically. The interface software program apart from graphic display also automatically saves the original digitized signals and the derived parameters in an excel format strip chart. This can be accessed for further analysis after experimentation.

A sample respiration pattern showing the computed indicators estimation schemes is presented in Figure 3. Respiration cycle was computed by counting the number of times the chest rose in a minute of testing and was correlated with the number of peaks recorded in the respiration pattern.

RC was measured via dividing 1 by the respiration time (t) (in seconds), i.e. time between successive RCs expressed as:

Figure 1 Flow chart of biometric identification system

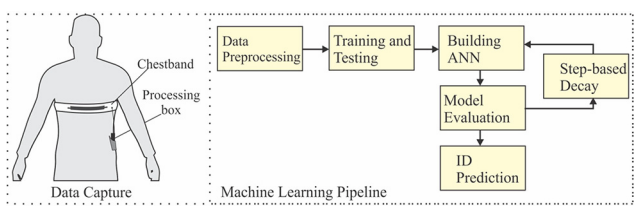

Figure 2 (a) Prototype smart chest band and (b) sensor software interface

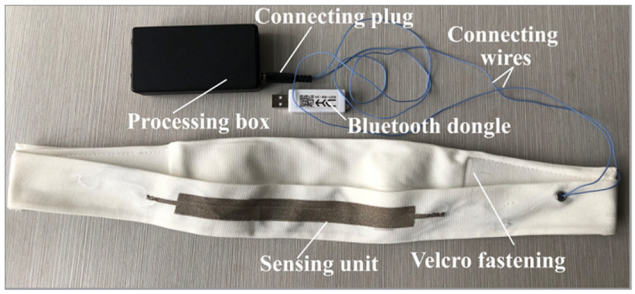

(a)

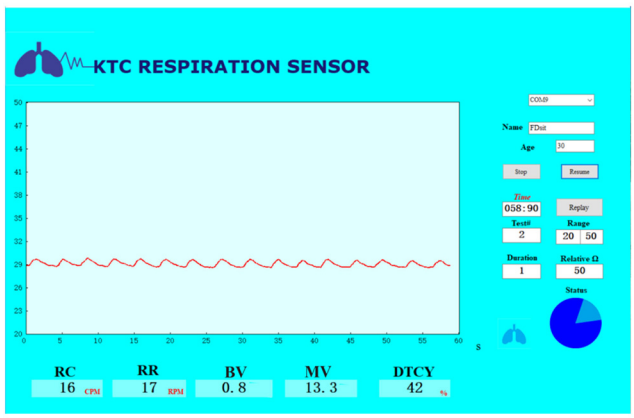

(b)

Figure 3 Sample respiration pattern showing indicator computation schemes

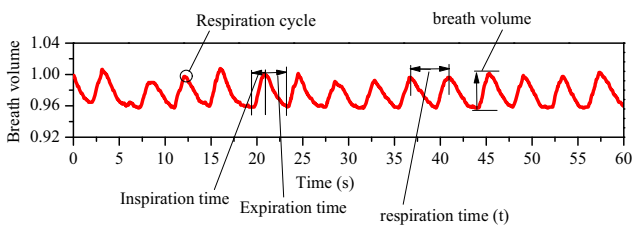

$$Respiration\ rate\ (RR) = \frac{1}{t} \quad (1)$$

The volume of gas inhaled or exhaled during the respiratory cycle is referred to as the BV in this study and has been estimated by measuring the peak value of each pattern cycle. MV was also calculated by:

$$Moment\ ventilation\ (MV) = RR \times BV \quad (2)$$

DTCY defines the ratio of inspiration to the total respiratory cycle (TI/Ttot) and is expressed as:

$$Inspiratory\ duty\ cycle\ (DTCY) = \frac{T_I}{T_I + T_E} = \frac{T_I}{T_{tot}} \times 100 \quad (3)$$

3.2 Feature distribution

When dealing with a set of data, often the first thing will be to get a sense of how the variables are distributed. Using the respirations software's saved data, the feature distribution (range of values and density) of the respiration patterns, RC, RR, DTCY, BV and MV variables for the biometric prediction system are shown in Figure 4. In the plots, it can be seen that the variables for respiration pattern and cycle are normally distributed, whereas RC appears to be jumbled up. Both BV and MV are conspicuously skewed to the left and DTCY is generally skewed to the right.

3.3 Data pre-processing

The first step of a machine learning model prediction process is to take care of data inadequacies which may include incompleteness, inconsistencies and or lacking definite behaviors or trends. All these inadequacies are likely to generate many errors. The processing step thus involves transforming raw data into an understandable format. Machine learning algorithm needs to distinguish the metrics of features and the dependent variable vector. Fortunately in the case of this study, all missing values were highly taken care of in the data collection stage which eases the burden of dealing with missing data. An operation which was considered vital is encoding categorical data. The data set has two categorical variables, the "activity" and the "subject" variable. With label encoder, we transformed these two variables into categorical variable. Finally, because the activity is part of the metrics of features X one hot encoding was performed on the variable. One hot encoding exponentially increases the number of features; hence, converting n levels to n-1 columns to prevent dummy variable trap.

3.4 Training and testing

The ANN algorithm generally follows the usual splitting method, thus 70 per cent for training instances and 30 per cent for testing instances for model 1, whereas for model 2 there are 60 per cent training instances, 20 per cent testing instances and 20 per cent validation instances (Choudhury and Greene, 2018). The final model was built using model 1 that contains 14,4359 training set and 61,869 test set. The pie chart below (Figure 5) shows the said splitting models. A random state of 101 was issued to ensure that the output of run 1 is equal to the output of run 2 and the subsequent runs. This was subsequently followed by engaging in min–max normalization to rescale the range of the metrics of features to the range between −1 and 1.

3.5 Building the artificial neural network

This section describes suitable training algorithm for the data set and determined the complexity of the model, which is the optimal number of neurons in the network. For optimum performance of the ANN model, a network with four hidden layers was implemented. The input and the first hidden layer initialize weight to small numbers close to zero. This was then followed by the first observation on the data set in the input layer where each feature is one input node. The number of nodes to be input in the network are the metrics of features. Hence, the first hidden layer is made up of 8 input parameters, with 62 neurons. The number of neurons was increased to 128

Figure 4 Feature distribution of the (a) respiration pattern, (b) respiration cycles, (c) respiration rate, (d) breath volume and (e) inspiration duty cycle variables from the sensor

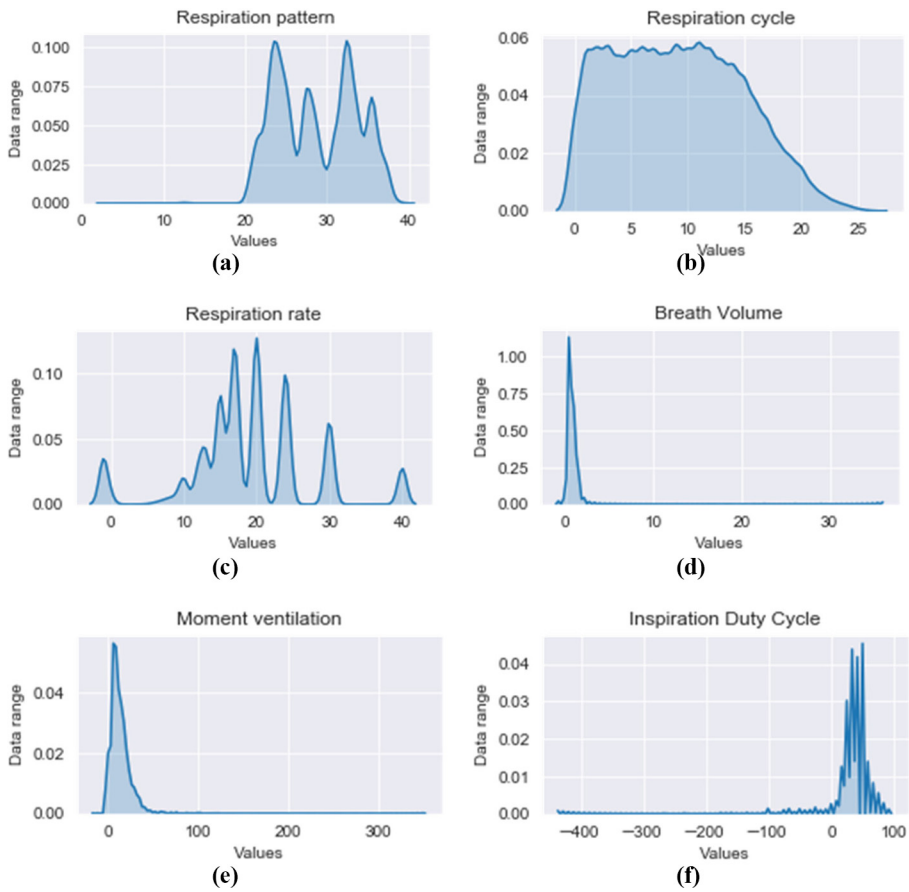

Figure 5 Model 1 shows the partitioned data of 70 per cent training instances and 30 per cent testing instances. Model 2 shows 60 per cent training instances, 20 per cent testing instances and 20 per cent validation instances

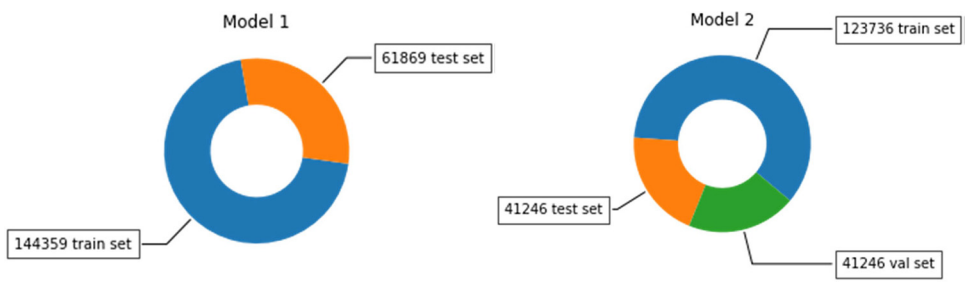

in the second hidden layer and 196 neurons in the third hidden layer. And 38 neurons in the fourth hidden layer and finally the output layer takes the same number as the metrics of features and output the probability as shown in Figure 6. This helps our algorithm to achieve a model with the best complexity to produce an adequate fit of the data.

Batch normalization was used to improve the performance and stability of artificial neural networks after the first hidden layer. To help combat underfitting and overfitting, a learning rate and drop factor was engaged while fitting the data to the model (see Section 6 learning rate). Batch learning with the size of 256 was used to hold the update of weights and biases until all the data records in the training data set were passed through the network and their associated changes of weights and biases computed and averaged.

For example, the data had 14,4359 training instances, with batch size = 256, meaning the algorithm initially takes 256 samples (from 1st to 256th) of the training data set to train the network. Followed by the second 256 samples (from 267th to 512th) and trains the network again. The process continues until all the training instances propagate through the network.

Figure 6 The ANN architecture and the corresponding layers

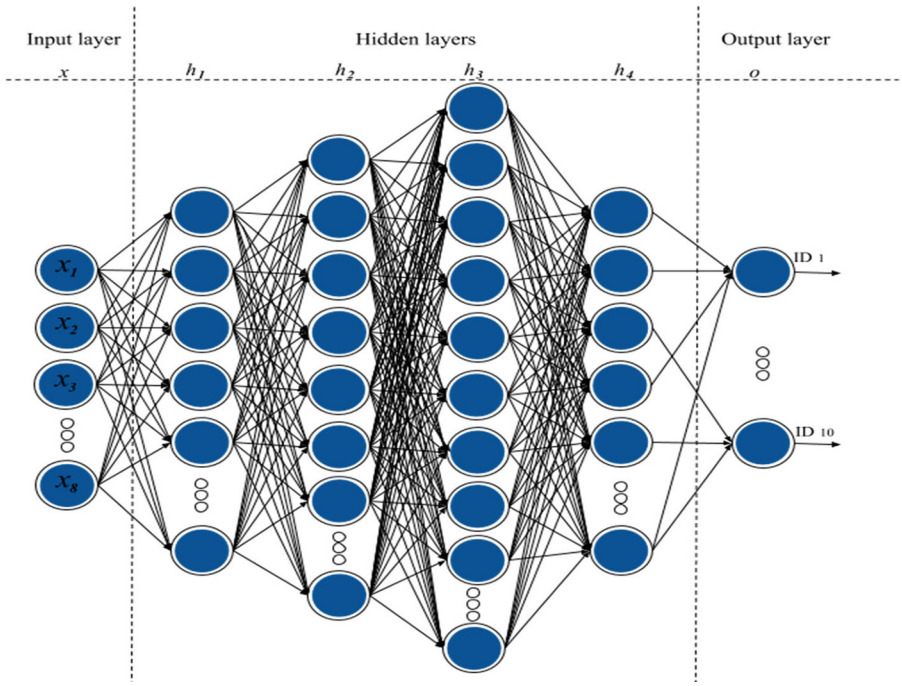

3.6 Learning rate

Learning rate α controls the steps a machine learning algorithm takes along the gradient. Higher α values imply that bigger steps were taken, whereas low values of α indicate tiny steps. During the training process, attempts were made to find some locations along the loss landscape where the network obtains reasonable accuracy. Consideration was not given to global or local minima, but practically, simply discovering an area of the loss landscape with acceptable low loss and high accuracy. The learning rate on an epoch-to-epoch basis was adjusted to minimize the loss and increase the model's accuracy.

To experiment with deferent values of learning rate, we engaged a step-based decay to systematically drop the learning rate after specific epochs during training. Our learning rate function is defined as:

$$\alpha = \alpha_{init} \times f^{(1+e)/d} \tag{5}$$

where α_{init} is our initial learning rate, f is the factor value controlling the rate at which the learning rate drops. e is the number of epochs to run and d is the drop in epoch's value. For example, if the initial learning rate of α = 0.01, then the learning rate will decrease over time using 50 epochs with a decay term 0.01/50. The learning rate decay was not only tuned to improve the model accuracy but also to lower the effects of overfitting; by this means, the chances of increasing the ability of the model to generalize are high. Table I exhibit the impact of learning rate decay factor on the prediction model. Even though both factors obtained a good accuracy of 0.9515 and 1.00 per cent, respectively, at epoch 50 the learning rate was very small at 5.82e-13 for factor = 0.25 and 3.91e-19 for factor = 0.5 and was unable to make any significant changes to the weights to influence the model loss and accuracy on the validation data. Finally, factor = 0.5 achieved lesser loss as compared to factor = 0.25. This implied a 5 per cent increment in accuracy from training without learning rate decay was also recorded.

Table I Experimenting with different learning rate decay factors

Learning rate decay factor	Learning rate (α)	Accuracy	Loss
Factor = 0.25	5.82e-13	0.9515	0.0869
Factor = 0.5	3.91e-19	0.98	0.0275

Also to see the reduction of loss and improvement of our classification accuracy in the lessen effect of overfitting; an ablation was performed on the model by training without learning rate decay. The experiment shows that learning rate decay indeed not only improves our model accuracy but also combats the effects of overfitting as shown in Figure 6. Notice how the training and validation curves with learning rate decay match each other nearly identical over the course of 100 epochs Figure 7(b). This implies that there is no occurrence of overfitting or issue with the training process. With a learning rate drop, (factor = 0.5), the network is able to continue to learn past epoch 40 until stagnation occurs which yielded a classification accuracy of 100 per cent. There is no dramatic increase in the gap between the training and validation loss.

Training and validation curves even though try to mimic each other on training loss and accuracy without learning rate decay as shown in Figure 7(a). There is fluctuation with spikes on the validation curves and the curves seem not to have stagnation even at epoch 100. It yielded a classification accuracy of 95 per cent and loss = 0.33, which may seem acceptable but suffers slightly overfitting. Due to the stagnation of the model past epoch 40 on training loss accuracy with learning rate decay, our final model was trained with 50 epochs.

Figure 7 (a) Training loss and accuracy without learning rate decay and (b) training loss and accuracy with learning rate decay

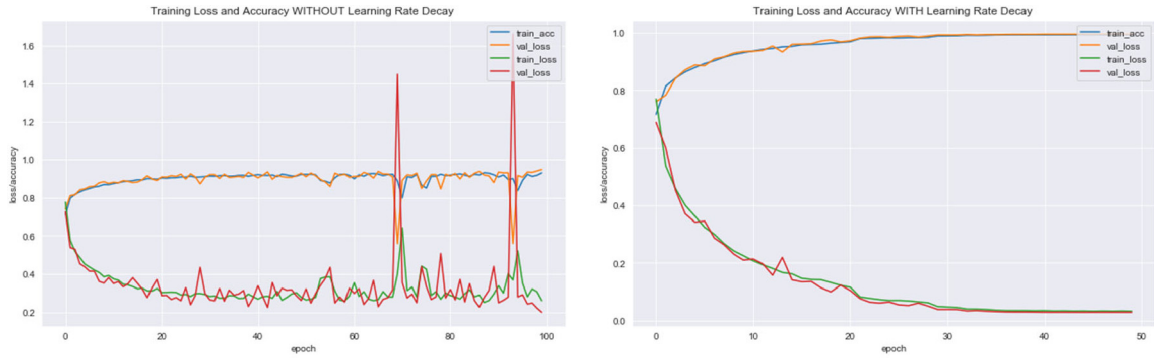

(a) (b)

Other parameters vital to the training model are L1/L2 regularization penalty of l1_l2 = 0.001 on our weights as regularization increases network testing accuracy at the expenses of training accuracy. And a random state variable (rSV = 101) on the train test split.

3.7 Fitting and evaluating the model

After designing the appropriate ANN model, it was deployed on our pre-processed data set and the accuracy performance measures were computed based on 50 epochs.

4. Results and discussion

The final model was run on 50 epochs with an initial learning rate of (lr = 0.01) and decay factor = 0.5 which yielded a classification accuracy of 98 per cent. Table II shows the training results obtained by the set parameters of the algorithm. They include final state from the neural network, the regularization penalty, random state variable of the training algorithm and threshold for prediction.

Regardless of how much data was used to test the trained algorithm, there was still the need to work out whether or not the result is good enough. Table III shows a confusion matrix of the correct and miss classifications prediction made by the ANN model on the testing data set based on a decision threshold of 0.5. The rows represent the target variables and the columns denote the output classes belonging to the testing data set. The diagonal cells depict the correctly classified and the off-diagonal cells indicate the misclassified instances.

The table shows 51,338 correctly classified instances out of 51,557 test set. This shows that only 169 misclassified instances have been recorded by the model. The description of systematic errors for the difference between a result and a

Table II Set parameters for the final ANN model

Parameters	Value
Initial learning rate (*lr*)	0.01
Decay factor (*factor*)	0.5
Regularization (*l1_l2*)	0.001
Random state variable (*rSV*)	101
Threshold (t)	0.5

Table III Confusion matrix of the correct and miss classification prediction

		Predicted class									
		0	**1**	**2**	**3**	**4**	**5**	**6**	**7**	**8**	**9**
True class	**0**	3568	0	0	0	0	0	30	0	4	0
	1	0	3618	0	0	0	4	0	2	0	0
	2	1	0	9192	0	0	0	2	0	0	0
	3	0	1	0	5110	0	3	0	2	0	11
	4	0	0	6	0	4014	0	0	0	0	0
	5	0	2	0	0	0	3898	0	1	0	2
	6	26	0	7	0	0	0	4182	0	2	0
	7	0	0	0	0	0	0	0	7083	15	9
	8	2	1	5	1	0	7	4	1	7789	0
	9	0	0	0	0	0	4	0	8	6	2961

"true" value was then calculated from the confusion matrix using the following equation:

$$acc = \frac{TP + TN}{TP + TN + FP + FN} \tag{6}$$

where true positive is true-positive, false positive is false-positive, true negative is true-negative prediction and false negative is false-negative prediction. Below is the accuracy precision on the final model.

As can be seen in Table IV, the ANN obtained an average classification accuracy of 98 per cent. Another important part in artificial neural networks is the loss function. To help measure the inconsistency between predicted value ($\hat{y}$) and the ground truth label (y), a computation of the mean squared error (MSE), mean absolute error (MAE) were carried out.

These quantities were used to measure how close the predictions are to the eventual outcomes, mean absolute percentage error (MAPE), a variant of MAE. These are non-negative values, where the robustness of the model increases along with the decrease of the value of loss function as shown in Figure 8.

Finally, cosine proximity of the predicted target was carried out. The cosine proximity loss computes the cosine proximity between the output of the network and the values supplied to the fit function. MSE works by taking the difference between

Table IV Precision (%) and recall (%) and F1-score of our ANN model performance

		"Participant"	
Subject	Precision	Recall	f1-score
0	0.94	0.91	0.93
1	0.98	0.99	0.99
2	0.98	0.99	0.98
3	0.99	0.98	0.98
4	0.99	0.98	0.99
5	0.99	0.99	0.99
6	0.96	0.97	0.97
7	0.98	0.99	0.98
8	0.99	0.98	0.98
9	0.98	0.97	0.98
Avg/total	0.98	0.98	0.98

each of the estimated and the real value, squaring them and dividing their sum by the number of samples and for the estimator to be a good model. A small MSE is better because it implies agreement between the prediction and the reality. From Figure 8 the MSE run on 50 epochs was very small between the range of 0.02 and 0.04 with an average of 0.03.

The RMSE is the square root of our MSE which is of 0.04. To measure the deviation from the actual data in terms of percentage, we went ahead to explore the MAPE, as shown in Figure 8, and the cosine proximity. They are good measures of errors and better measures of goodness-of-fit than a correlation coefficient or confusion matrix. By these, the chance of increasing the ability of our model to generalize is high.

Receiver operating characteristic curve (ROC) is plotted using the true positive rate (TPR) against the false positive rate (FPR) for the different possible cut points of our observations test.

The TPR, also referred to sensitivity or recall, is used to measure the percentage of actual positives which are correctly identified, whereas samples incorrectly classified as positive are referred to as FPR (Wang and Zheng, 2013). ROC shows the trade-off between sensitivity and specificity. That is, any increase in sensitivity will be accompanied by a decrease in specificity (Tape, 2018). The slope of the tangent line at a cut point gives the likelihood ratio for that value of the test.

From Figure 9, it can be observed that the curves follow the top left upper border and the closer to the top border of the ROC space, the more accurate the test. The closer the curve comes to the 45° diagonal of the ROC space, the less accurate the test; hence, none of our test falls in that range. The ROC presented in Figure 8 shows a 98 per cent TPR. This high accuracy justifies the hypothesis that respiratory patterns are unique for every individual. Our 98 per cent accuracy result exceeds the results obtained by (Li *et al.*, 2020) and also compares favourably with the high accuracy rates obtained by (Zhao *et al.*, 2018; Hammad *et al.*, 2019) in their studies on biometric identification via related ECG signals.

Figure 9 ROC curve of predicted results

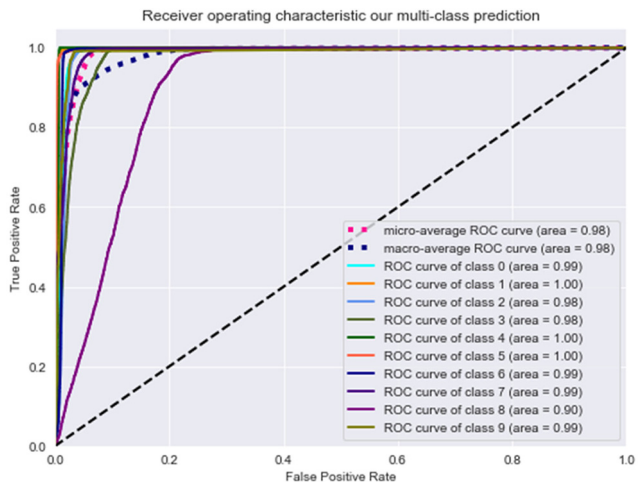

Figure 8 (a) Mean squared error, (b) mean absolute error, (c) mean absolute percentage error and (d) cosine proximity

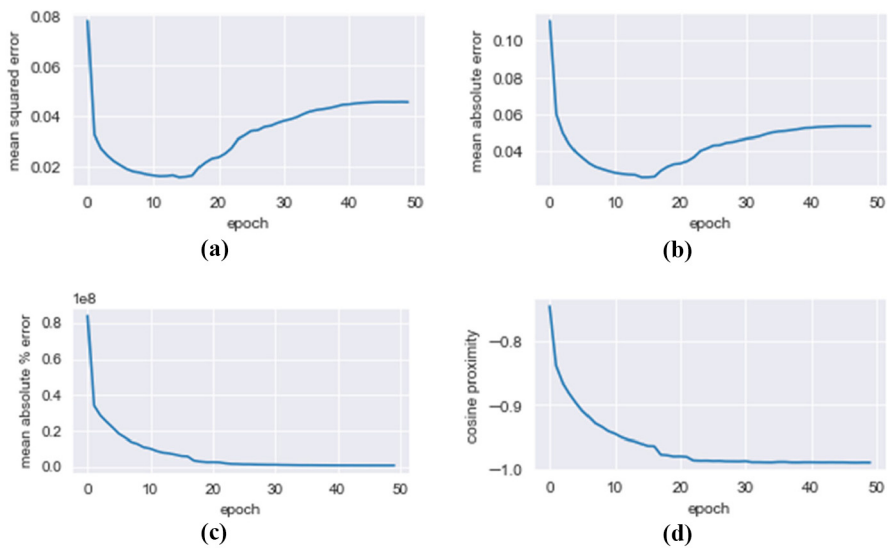

This proposed system has an advantage over conventional multimodal biometric systems that combine different biometric features, in that with this system, only a single device is required to extract multiple features. Respiratory rate when compared with other physiological features such as ECG, only a simple device such as smart band or smart bra is needed for enrolment as demonstrated in this proposed system. Respiratory pattern biometrics also satisfies the universality criteria expected of biometric features – the respiratory pattern feature applies to every person as breathing is the basis of life.

5. Conclusion

This study presented the use of respiration pattern data obtained from our knitted smart chest band respiration device for biometric prediction system. The results establish that breath patterns, just like the other known physiological signals, such as ECG and EEG, can be used as biometric feature.

Experimental results using the ANN model showed that out of 51,338 test set, 51,557 came out as correctly classified instances. This shows that only 169 misclassified instances have been recorded by the model. The final model run on 50 epochs with an initial learning rate of (lr = 0.01) and decay factor = 0.5 yielded a classification accuracy of 98.00 per cent. Also, the overall performance of the system was also impressive with an average classification accuracy of 98.00 per cent. There was also a 5 per cent increment in accuracy from training without learning rate decay.

This experiment shows that data adduced from other wearable strain sensors can be processed using ANN models and other machine learning algorithms not only for biometric prediction systems but also for other human activity recognition applications. This success of this study in our opinion should be an impetus for possible studies in the application of chest breathing sensors for human machine interfaces for assisting rehabilitation and entertainment applications.

References

Akhter, N., Tharewal, S., Kale, V., Bhalerao, A. and Kale, K. V. (2016), "Heart-based biometrics and possible use of heart rate variability in biometric recognition systems", in Chaki, R., Cortesi, A., Saeed, K. and Chaki, N. (Eds), *Advanced Computing and Systems for Security*, Vol. 1, Springer, New Delhi.

Biel, L., Pettersson, O., Philipson, L. and Wide, P. (2001), "ECG analysis: a new approach in human identification", *IEEE Transactions on Instrumentation and Measurement*, Vol. 50 No. 3, pp. 808-812.

Campisi, P. and Rocca, D.L. (2009), "EEG biometrics", in Li, S.Z. and Jain, A.K. (Eds), *Encyclopedia of Biometrics*, Springer, Boston, MA.

Cheema, A. and Singh, M. (2019), "Psychological stress detection using phonocardiography signal: an empirical mode decomposition approach", *Biomedical Signal Processing and Control*, Vol. 49, pp. 493-505.

Choudhury, A. and Greene, C.M. (2018), "Prognosticating autism spectrum disorder using artificial neural network: Levenberg-Marquardt algorithm", *Journal of Bioinformatics and Systems Biology*, Vol. 1 No. 1, pp. 1-10.

Duke, J. (2011), "CHAPTER 24 - capnography", in Duke, J. (Ed.), *Anesthesia Secrets*, 4th ed., Mosby, Philadelphia.

Gilady, E., Lindskog, D. and Aghili, S. (2014), "Intent biometrics: an enhanced form of multimodal biometric systems", *2014 28th International Conference on Advanced Information Networking and Applications Workshops, 13-16 May 2014*, pp. 847-851.

Hammad, M., Zhang, S. and Wang, K. (2019), "A novel two-dimensional ECG feature extraction and classification algorithm based on convolution neural network for human authentication", *Future Generation Computer Systems*, Vol. 101, pp. 180-196.

Khuwaja, G.A. (2006), "A multimodal biometric identification system using compressed finger images", *Cybernetics and Systems*, Vol. 37 No. 1, pp. 23-46.

Kirson, L.E. and Koltes-Edwards, R. (2011), "CHAPTER 23 - pulse oximetry", in Duke, J. (Ed.), *Anesthesia Secrets*, 4th ed., Mosby, Philadelphia.

Lapi, S., Lavorini, F., Borgioli, G., Calzolai, M., Masotti, L., Pistolesi, M. and Fontana, G.A. (2014), "Respiratory rate assessments using a dual-accelerometer device", *Respiratory Physiology & Neurobiology*, Vol. 191, pp. 60-66.

Li, Y., Pang, Y., Wang, K. and Li, X. (2020), "Toward improving ECG biometric identification using cascaded convolutional neural networks", *Neurocomputing*, Vol. 49, pp. 24-33.

Macwan, R., Benezeth, Y. and Mansouri, A. (2019), "Heart rate estimation using remote photoplethysmography with multi-objective optimization", *Biomedical Signal Processing and Control*, Vol. 49, pp. 24-33.

Mimoz, O., Benard, T., Gaucher, A., Frasca, D. and Debaene, B. (2012), "Accuracy of respiratory rate monitoring using a non-invasive acoustic method after general anaesthesia", *British Journal of Anaesthesia*, Vol. 108 No. 5, pp. 872-875.

Raji, R.K., Miao, X., Wan, A., Niu, L., Li, Y. and Boakye, A. (2019), "Knitted piezoresistive smart chest band and its application for respiration patterns assessment", *Journal of Engineered Fibers and Fabrics*, Vol. 14, pp. 1-14.

Rétory, Y., David, P., De Picciotto, C., Niedzialkowski, P., Bonay, M. and Petitjean, M. (2017), "Validity of thoracic respiratory inductive plethysmography in high body mass index subjects", *Respiratory Physiology & Neurobiology*, Vol. 242, pp. 52-58.

Ring, T. (2015), "Spoofing: are the hackers beating biometrics?", *Biometric Technology Today*, Vol. 2015 No. 7, pp. 5-9.

Sharpton, R.A., Yu, F.S. and Shoair, O.A. (2019), "Comparison of pharmacy students' perceptions and attitudes toward spirometry first-hand experience versus paper-based active learning", *Currents in Pharmacy Teaching and Learning*, Vol. 11 No. 2, pp. 192-197.

Sibai, F.N., Hosani, H.I., Naqbi, R.M., Dhanhani, S. and Shehhi, S. (2011), "Iris recognition using artificial neural networks", *Expert Systems with Applications*, Vol. 38 No. 5, pp. 5940-5946.

Singh, Y.N., Singh, S.K. and Gupta, P. (2012), "Fusion of electrocardiogram with unobtrusive biometrics: an efficient individual authentication system", *Pattern Recognition Letters*, Vol. 33 No. 14, pp. 1932-1941.

Tape, T.G. (2018), "ROC curves", University of Nebraska Medical Center, available at: http://gim.unmc.edu/dxtests/roc2.htm (accessed 13 February 2019).

Wang, H. and Zheng, H. (2013), "True positive rate", in Dubitzky, W., Wolkenhauer, O., Cho, K.-H. and Yokota, H. (Eds) *Encyclopedia of Systems Biology*, Springer, New York, NY.

Wilkinson, J.N. and Thanawala, V.U. (2009), "Thoracic impedance monitoring of respiratory rate during sedation – is it safe?", *Anaesthesia*, Vol. 64 No. 4, pp. 455-456.

Zhao, Z., Zhang, Y., Deng, Y. and Zhang, X. (2018), "ECG authentication system design incorporating a convolutional neural network and generalized S-transformation", *Computers in Biology and Medicine*, Vol. 102, pp. 168-179.

Corresponding author

Rafiu King Raji can be contacted at: mrkingraji@outlook.com

For instructions on how to order reprints of this article, please visit our website:
www.emeraldgrouppublishing.com/licensing/reprints.htm
Or contact us for further details: **permissions@emeraldinsight.com**